RESEARCH ARTICLE

Impact of solar geoengineering on temperatures over the Indonesian Maritime Continent

Heri Kuswanto[1,2] 🟢 | Ben Kravitz[3,4] | Brina Miftahurrohmah[5] | Fatkhurokhman Fauzi[6] | Ardhasena Sopahaluwaken[7] | John Moore[8]

[1]Centre for Disaster Mitigation and Climate Change, Institut Teknologi Sepuluh Nopember, Surabaya, Indonesia

[2]Department of Statistics, Institut Teknologi Sepuluh Nopember, Surabaya, Indonesia

[3]Department of Earth and Atmospheric Sciences, Indiana University, Bloomington, Indiana, USA

[4]Atmospheric Sciences and Global Change Division, Pacific Northwest National Laboratory, Richland, Washington, USA

[5]Department of Information System, Universitas International Semen Indonesia (UISI), Gresik, Indonesia

[6]Department of Statistics, Universitas Muhammadiyah Semarang, Semarang, Indonesia

[7]Agency for Meteorology, Climatology and Geophysics (BMKG), Jakarta, Indonesia

[8]College of Global Change and Earth System Science, Beijing Normal University (BNU), Beijing, China

Correspondence
Heri Kuswanto, Center for Disaster Mitigation and Climate Change, Institut Teknologi Sepuluh Nopember, Surabaya, Indonesia.
Email: heri_k@statistika.its.ac.id

Abstract

Climate change has been projected to increase the intensity and magnitude of extreme temperature in Indonesia. Solar radiation management (SRM) has been proposed as a strategy to temporarily combat global warming, buying time for negative emissions. Although the global impacts of SRM have been extensively studied in recent years, regional impacts, especially in the tropics, have received much less attention. This article investigates the potential stratospheric sulphate aerosol injection (SAI) to modify mean and extreme temperature, as well as the relative humidity and wet bulb temperature (WBT) change over Indonesian Maritime Continent (IMC) based on simulations from three different earth system models. We applied a simple downscaling method and corrected the bias of model output to reproduce historical temperatures and relative humidity over IMC. We evaluated changes in geoengineering model intercomparison project (GeoMIP) experiment G4, an SAI experiment in 5 Tg of SO_2 into the equatorial lower stratosphere between 2020 and 2069, concurrent with the RCP4.5 emissions scenario. G4 is able to significantly reduce the temperature means and extremes, and although differences in magnitude of response and spatial pattern occur, there is a generally consistent response. The spatial response of changes forced by RCP4.5 scenario and G4 are notably heterogeneous in the archipelago, highlighting uncertainties that would be critical in assessing socio-economic consequences of both doing, and not doing G4. In general, SAI has bigger impacts in reducing temperatures over land than oceans, and the southern monsoon region shows more variability.

G4 is also effective at reducing the likelihood of WBT > 27°C events compared with RCP4.5 after some years of SAI deployment as well as during the post-termination period of SAI. Regional downscaling may be an effective tool in obtaining policy-relevant information about local effects of different future scenarios involving SAI.

1 | INTRODUCTION

Indonesia, and the Maritime Continent in general, are known to be some of the most vulnerable regions to climate change, largely because it is an archipelago, with densely populated regions vulnerable to coastal flooding, and also forested and intensively farmed interiors susceptible to fire and drought (Measey, 2010). In addition to the flood and tropical storm risks, Indonesia is especially vulnerable to extreme temperature changes; extreme heat is a major cause of disasters in Indonesia, leading to droughts and fires. Fernades *et al.* (2017) found an increasing trend of drought and wildfire risk in Indonesia, a fact that has been confirmed by the Indonesian National Disaster Management Agency (BNPB) in its Disaster Indices Report (BNPB, 2019). The impacts of warming temperatures and precipitation change also make it difficult for Indonesia to meet food demand as livelihoods are directly affected. Urban heat and humidity rise under greenhouse gas scenarios are projected to hugely impact liveability in, for example, Jakarta (Varquez *et al.*, 2020). Examining future trends in these changes are crucial for understanding and ultimately addressing climate change in Indonesia.

Solar radiation management (SRM), sometimes known as solar geoengineering, has been proposed as a potential strategy to temporarily combat global warming (Crutzen, 2006; Wigley, 2006; NRC, 2015). There are many proposed techniques, but the most commonly discussed SRM method is via stratospheric sulphate aerosol injection (SAI), which is based on observations that past volcanic eruptions cool the planet (Budyko, 1977; Crutzen, 2006). There has been much research over the past decade into the climate impacts of SAI. Numerous studies have shown that SAI would likely reduce impacts of climate change on global temperatures (Govindasamy and Caldeira, 2000; NRC, 2015), precipitation (Tilmes *et al.*, 2013), extreme events (Curry *et al.*, 2014; Ji *et al.*, 2018), the cryosphere (Moore *et al.*, 2010) and numerous other areas. However, SAI is not without its side effects; in a recent review, Irvine *et al.* (2017) pointed out the potential risks of SAI techniques as compared with risks posed by climate change. Recently, more studies have focused on investigating SAI impacts such as on agriculture (Pongratz *et al.*, 2012; Xia

et al., 2014; Yang *et al.*, 2016; Proctor *et al.*, 2018), public health (Effiong and Neitzel, 2016), biodiversity (Trisos *et al.*, 2018), hydrology (Dagon and Schrag, 2016) and economics (Harding *et al.*, 2020), among others.

Most of the aforementioned studies have attempted to investigate SAI impacts on future climate conditions on regional and global scale. Ricke *et al.* (2010) found that SAI would generally lead to less extreme temperature and precipitation anomalies, but they found significant diversity in climate response to SAI on a regional scale. Numerous studies since then have found that, while moderate amounts of geoengineering show promise in alleviating many aspects of climate change in most regions, there are for some regions and climate fields, cases where SAI exacerbates climate change (Kravitz *et al.*, 2014; Irvine *et al.*, 2019). Because most studies of SAI have been conducted by researchers in the global north, many of the conclusions obtained from SAI inherently are biased toward this viewpoint. In contrast, people in the global south are on the front line of climate change (ADB, 2019), and in the context of SRM, developing countries have the most to gain or lose. Increasing informed global south participation in SRM research has strong potential to enrich discussions around SRM and reduce that bias (Rahman *et al.*, 2018). To date, research on the impacts of SRM on developing countries by developing country researchers is still very limited. Of the few studies, Pinto *et al.* (2020) showed that SAI is effective in reducing mean and extreme temperature but not effective in maintaining rainfall to historical values over South Africa. Karami *et al.* (2020) finds that SRM could partially offset the shift of storm tracks induced by global warming, and thus reduce some water stresses in the Middle East. Furthermore, Da-Allada *et al.* (2020) studied how SRM could affect the West African monsoon, concluding that SRM would reduce climate-caused disruptions to rainfall in the northern and southern Sahel.

Here we continue this effort to increase developing country participation in SRM research. This article is, to the best of our knowledge, the first investigation of SAI impacts on Indonesia, particularly the ability of SAI to offset temperature changes in the Indonesian Maritime Continent due to climate change. The IPCC Fifth Assessment Report (IPCC;, 2014) reports that under an RCP4.5 scenario,

tropical countries such as Indonesia will experience long-term warming with the projected temperature change to mid-century (2046–2065) exceeding 2.5°C. Supari *et al.* (2017) analysed the observed changes in extreme temperature and precipitation over Indonesia and found that the annual means of daily maximum (TX_{mean}) and minimum temperature (TN_{mean}) had increased significantly by 0.18 and 0.30°C per decade, respectively. In general, they found significant warming trends in extreme temperature indices. Our aims are to improve understanding for the research community, stakeholders, and the general public of the Maritime Continent as to what SRM might mean for them. Moreover, this information will be crucial for understanding how Indonesia may be able to address climate change.

Most studies of climate change in Indonesia, and all studies of SRM that have made conclusions about the Maritime Continent, have been performed with Earth System Models (ESMs) (e.g., Faqih *et al.*, 2016; Sarmini and Faqih, 2016; Ji *et al.*, 2018; Parkhurst *et al.*, 2019). However, ESMs are of too coarse a resolution to explain regional or local climate characteristics, and are often biased compared with historical observations. To carry out regional impact studies, we perform downscaling and bias correction over the Indonesian Maritime Continent to the ESM outputs using state-of-the-art methods to ensure the quality and validity of climate projections of SAI experiments. The downscaling generates high-resolution regional climate information based on the large-scale information from the ESM (Trzaska and Schnarr, 2014; Tang *et al.*, 2016; Zhang *et al.*, 2020). Furthermore, our analysis focuses on investigating the geographic pattern of changes over the Indonesian Maritime Continent.

The structure of this article is organized as follows. A detailed description about the dataset analysed in this article as well as the downscaling and bias correction methods are given in Section 2. Section 3 provides the results of the downscaling and bias correction, continued with the impact analysis, and Section 4 contains discussion and conclusions from our study.

2 | DATA AND METHODOLOGY

2.1 | Data description

This study is focused on investigating SAI (as specified by the G4 scenario) impacts over the Indonesian Maritime Continent, (6°N–11°S, 95°E–141°E). For this study, we downscaled daily surface air temperature output as well as relative humidity from ESMs for the historical period and assessed future climates under both the Representative Concentration Pathway 4.5 (RCP4.5; Meinshausen *et al.*, 2011)

scenario alone and the G4 combined RCP4.5 and SAI scenario. The RCP4.5 simulation includes of change in greenhouse gases and aerosols such that the net radiative forcing in the year 2,100 is 4.5 W m^{-2} as compared with the preindustrial era. The SAI scenario is the GeoMIP experiment G4 (Kravitz *et al.*, 2011), which is based on RCP4.5 with the addition of 5 Tg SO$_2$ per year injected continuously above the equator into lower stratosphere (16–25 km in altitude) beginning in 2020 until 2069. SAI is then terminated, and the simulation is run for an additional 20 years with standard RCP4.5 forcing to quantify the climate rebound. The RCP4.5 data is part of the Coupled Model Intercomparison Project Phase 5 (CMIP5; Taylor *et al.*, 2012) and is readily available via the Earth System Grid Federation (http://cmip-pcmdi.llnl.gov/cmip5/). This article investigates the performance or skill of three different ESMs that performed these simulations: BNU-ESM (Ji *et al.*, 2014), MIROC-ESM and MIROC-CHEM-ESM (Watanabe *et al.*, 2008, 2011). All three models have a horizontal resolution of 2.8° latitude and longitude. The two MIROC models are the same but for a more sophisticated atmospheric chemistry simulation in MIROC-ESM-CHEM. BNU-ESM has a lower atmosphere upper bound at 3 hPa (about 30 km), whereas the two MIROC models extend to 0.003 hPa in altitude (about 40 km). All three models represent stratospheric aerosol geoengineering using prescribed aerosol optical depth. In addition, MIROC-ESM-CHEM calculates aerosol surface area density based on the aerosol optical depth, for use in heterogeneous chemistry calculations. The land surface, vegetation, ocean, and sea ice components differ markedly between BNU-ESM and the two MIROC models. This study is focused on examining these three models which were the only ones with the necessary data for all of the experiments we investigated.

We evaluate the performance of downscaling and bias correction using three different methods on the historical period 1950–2005. We then use the best method to bias-correct future projections of ESM scenarios. We choose two periods: 2020–2069 and 2070–2089, representing the mid-century and end-century projection periods. For G4, 2069 is when SAI terminates, so the analysis of SAI under G4 is restricted to years prior to termination. The baseline for downscaling the historical period is the Modern-Era Retrospective Analysis for Research and Applications (MERRA) reanalysis dataset developed by Rienecker *et al.* (2011). The term "reanalysis" hereafter refers to MERRA-2 reanalysis data. The reanalysis data span from 1980 to early 2019. The datasets used to extract surface temperature and relative humidity are given in Table 1.

Furthermore, from the surface air temperature (°C) and relative humidity (%), we derived several variables to be analysed such as mean temperature (T_{mean}), maximum temperature (T_{max}), warm spell duration index (WSDI) and

TABLE 1   Summary of datasets used in the analysis

Data	Institution	Resolution	Scale	Scenario
MERRA reanalysis	NASA	0.625° × 0.625°	Daily	–
BNU-ESM	Beijing Normal University	2.8° × 2.8°	Daily	G4, RCP4.5
MIROC-ESM-CHEM	JAMSTEC	2.8° × 2.8°	Daily	G4, RCP4.5
MIROC-ESM	JAMSTEC	2.8° × 2.8°	Daily	G4, RCP4.5

wet bulb temperature (WBT). From this point forward, "temperature" refers to "surface air temperature."

2.2 | Downscaling and bias correction of ESM outputs

All ESM output (RCP4.5 and G4) were bias corrected and downscaled to the resolution of the reanalysis dataset (69.5 km). Moreover, to ensure the quality and validity of the projection, we examined three different bias correction methods: quantile delta mapping (QDM), bias correction constructed analogues with quantile mapping (BCCAQ) and the trend preserving bias correction method used in the inter-sectoral impact model intercomparison project (ISIMIP) approach, which is referred to as the ISIMIP method hereafter. The bias correction methods are applied to the downscaled data using "Climate Imprints" developed by Hunter and Meentemeyer (2005). The "ClimDown" R package (Cannon et al., 2016) was used to downscale the ESM outputs to the specified spatial resolution.

Quantile mapping (QM) based methods were chosen because of their ability to handle higher-order moments in addition to being computationally efficient (Wood et al., 2004; Piani et al., 2010; Gudmundsson et al., 2012; Teutschbein and Seibert, 2012). These methods are also simple to apply and do not require any assumptions about the shape of the distribution of the underlying variable. The QM method assumes that the distribution of simulated or estimated data preserves the distribution of any observed data. Some previous works that have been successfully applied QDM and/or BCCAQ are Sunyer et al. (2012), Sarr et al. (2015), Switanek et al. (2017), Lanzante et al. (2019) and Heo et al. (2019), among others. Werner and Canon (2016) specifically discussed the intercomparison of multiple gridded statistical downscaling methods (including QDM and BCCAQ) applied to hydrological extremes. Brief descriptions of each method are given as follows.

2.2.1 | Quantile delta mapping

The QDM was introduced by Cannon et al. (2015) and has been proven to be superior to the traditional quantile mapping method. This method uses the idea of quantile mapping (Panofsky and Brier, 1968) to preserve the changes in individual quantiles in general but not changes in the mean through the following formula:

$$D_f(x) = M_f(x) + \left\{ F_{O_h}^{-1}\left[M_f(M_f(x))\right] - F_{M_h}^{-1}\left[F_{M_f}(M_f(x))\right] \right\}$$

where, $D_f(x)$ is the bias corrected data in the future period, $F(\cdot)$ is the cumulative distribution function (CFD) with $F^{-1}(\cdot)$ as the inverse, O_h and M_h are reanalysis data and the raw model outputs in the historical period, respectively. Index h refers to "historical" and f indicates the "future" projection of the model simulations.

2.2.2 | Bias correction/constructed analogues with quantile mapping reordering

The BCCAQ is a constructed analogues downscaling approach where the bias correction of the large scale temperature is done by quantile mapping. This method entails building a constructed analogue (CA), or a library of observed daily coarse-resolution and corresponding high-resolution climate patterns of the variable to be downscaled (Hidalgo et al., 2008). Daily data are downscaled by selecting 30 days from the library that have the closest similarity to a given simulated day. Ridge regression is applied to determine the optimal weights that will be used to combine the 30 corresponding fine-scale library patterns (Maurer et al., 2010). Then bias correction of the climate analogue is performed by quantile mapping (Hunter and Meentemeyer, 2005).

2.2.3 | Intersectoral impact model intercomparison project

ISIMIP is one of the most popular bias correction approaches used in impact analysis. The ISIMIP method (Hempel et al., 2013) has been previously applied by Moore et al. (2019) and Chen et al. (2020) to correct the bias of CMIP5 and GeoMIP outputs. ISIMIP is designed

to preserve the long-term absolute (relative) trend in the ESM simulated data by modifying the daily variability of the simulated data about their monthly means to match the variability of the daily observation. A normal probability density function is assumed, and hence the method does not utilize quantile mapping ideas. Mapping of the simulated to observed temperature or relative humidity can be done by simply fitting linear regression (Hempel et al., 2013).

3 | RESULTS

3.1 | Skill evaluation of bias correction methods

We begin the discussion by evaluating the results of downscaling and bias correction of temperature data. Relative humidity results are provided in the Appendix S1.- Figure 1 depicts the annual mean temperature (land and sea combined over IMC) plots of the raw model outputs generated under three different G4 models and the all-model average, as well as reanalysis data for the periods of historical reference (1950–2005). Raw model output refers to the model outputs that have not been downscaled and bias corrected. We can see that the raw model outputs have a relatively large spread, indicating bias that needs to be corrected. However, among those three models, the BNU-ESM model has lower bias than MIROC models, which tend to underestimate the temperature reanalysis data. The lower panel of the figure depicts the data after downscaling and bias correction using QDM. We provide the plots after downscaling and bias correction with BCCAQ and ISIMIP in the Appendix S1 (Figures 1 and 2) as the pattern is quite similar to results using QDM. After bias correction, we observe good agreement on the annual pattern of the mean temperature among the model outputs and observations. The models have low spread and resemble the observations well with only few periods where the ensemble mean of the model deviates from reanalysis data significantly. The MIROC-ESM-CHEM model overestimates reanalysis in the early periods, but it tends to underestimate the reanalysis after approximately 20 years. The two other models (BNU-ESM and MIROC-ESM) tend to underestimate the observations in the 1980s–2000s. Overall, downscaling and bias correction are effective in obtaining a high resolution downscaled dataset with lower bias.

The BNU-ESM model had the lowest bias overall, and Figure 2 shows the spatial pattern of the bias for the corrected model outputs resulting from QDM. The bias in this case indicates how much the bias-corrected data deviates from the reanalysis. From the figure, we observe that the bias over land area is higher than over sea, reaching about 0.5°C, particularly over both land and sea in the eastern part of the domain. The three bias correction methods generate similar patterns over the region. We estimated the correlation between reanalysis data and bias corrected data at all 2,625 grid points to evaluate bias correction performance, finding that the bias correction methods perform equally well and all models are extremely good at capturing the spatial patterns of the observations indicated by significant correlations between reanalysis and bias corrected data over all grids. The total absence of stippling in Figure 2 indicates that correlations at all grids are statistically significant at the 95% level.

The skill of the bias correction methods applied to three different model outputs can be accessed via a Taylor diagram (Taylor et al., 2012). The diagram shows the correlation between reanalysis and bias corrected series relative to the root mean square difference. It provides a way of graphically summarizing how closely a pattern (or a set of patterns) matches observations (in this case, reanalysis data). The correlation performed in Taylor diagram measures the temporal correlation between daily temperature of the bias corrected series with reanalysis data averaged over the Maritime Continent. Taylor diagrams used to evaluate the performance (skill) of the bias correction methods are depicted in Figure 3 both on an annual and seasonal basis.

The Taylor diagram indicates that QDM outperforms BCCAQ and ISIMIP by showing higher correlation and lower mean square error. The correlation of QDM is around 0.6, while the correlations of BCCAQ and ISIMIP are slightly lower. Although QDM performs the best, and ISIMIP is the least skilful approach, skill differences are small among the methods with relatively equal correlation values. Furthermore, the seasonal based performance suggests that the methods have relatively low skill in correcting the bias of temperature during the wet season in Indonesia (DJF and MAM). The skill of the methods significantly increases during the dry season (JJA and SON). This improvement in skill reflects the small variability of daily temperatures during the dry season in Indonesia, and hence the importance of precipitation regimes in determining reliability of temperature forecasts.

Bias correction performance for relative humidity is broadly consistent with temperature (Figures S3 to S5). From the Taylor diagram of relative humidity (Figure S6), we see that ISIMIP produces the smallest RMSE. However, the correlations between reanalysis and the bias corrected output for all models are very low. The BCCAQ seems to have the lowest skill indicated by low correlation, high RMSE and standard deviation. The bias correction using
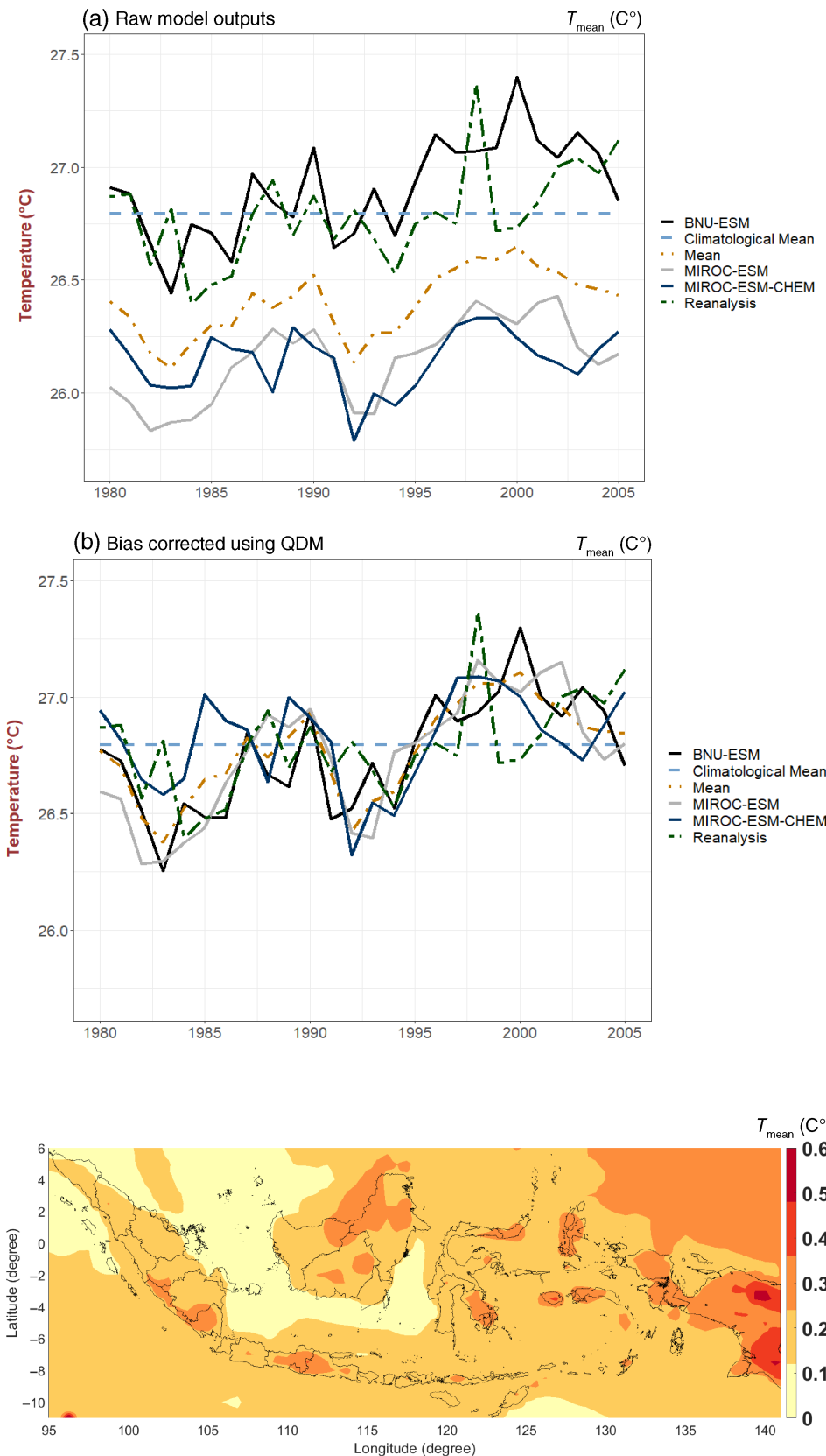
(a) Raw model outputs T_{mean} (C°)

(b) Bias corrected using QDM T_{mean} (C°)

FIGURE 1 Annual mean surface temperature (T_{mean}) plots of reanalysis data, raw outputs of three ESM models and its mean (a) and the bias corrected outputs using QDM (b). The 1980–2005 mean temperature (26.8°C, dashed line) is calculated over both land and sea of Indonesia Maritime Continent [Colour figure can be viewed at wileyonlinelibrary.com]

FIGURE 2 Map of absolute bias between reanalysis and bias corrected model outputs of mean temperature for the BNU-ESM model using QDM. The mean temperature is calculated over historical period (1950–2005) [Colour figure can be viewed at wileyonlinelibrary.com]

ISIMIP might reflect underdispersion of the corrected output. The QDM method gives modest performance in term of the RMSE, however, the correlations are significantly higher than those produced by ISIMIP and BCCAQ. Therefore, we prefer QDM to correct the bias of RCP4.5 and G4 series. Hence, all analyses in the following sections are
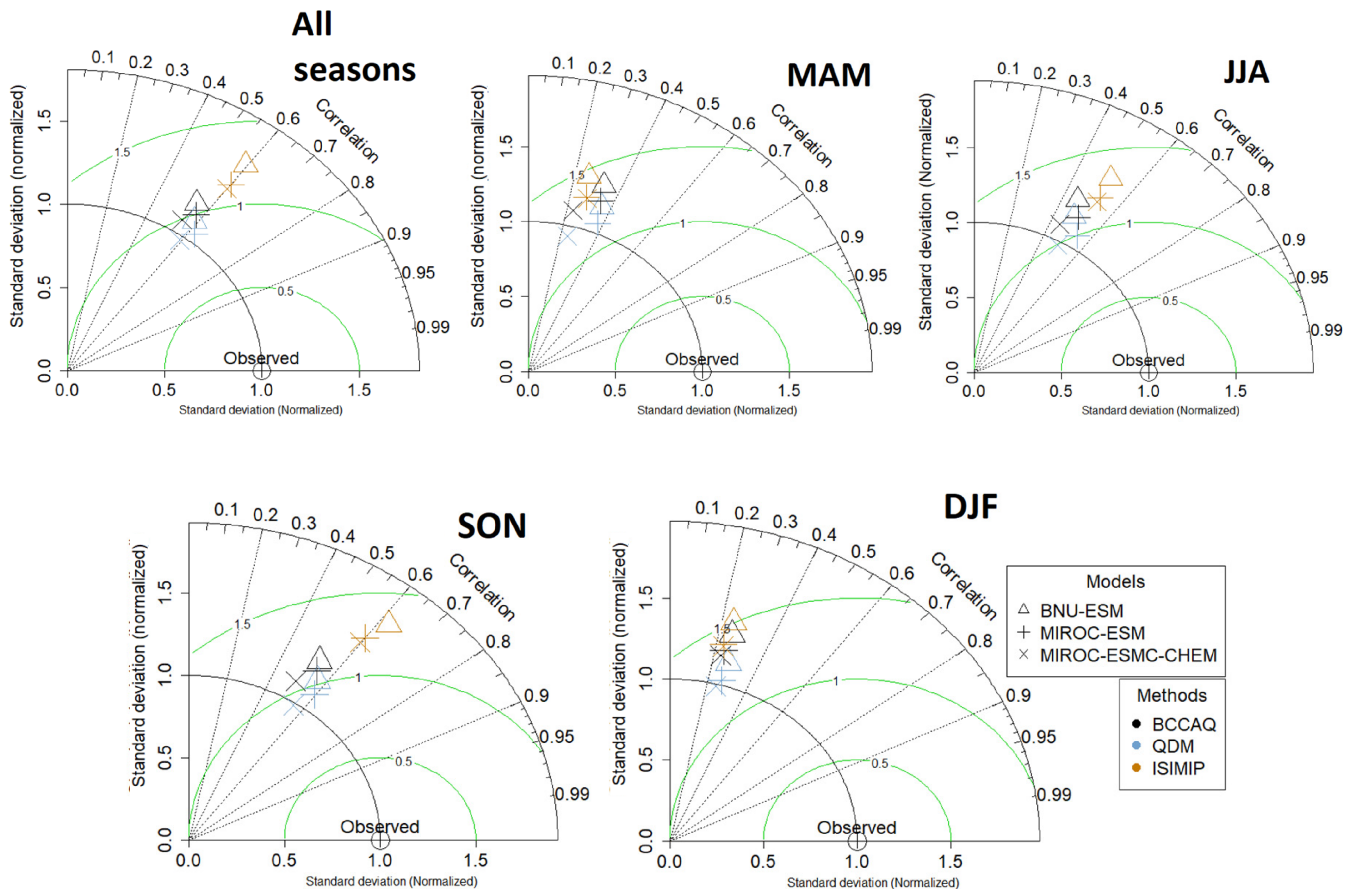
FIGURE 3   Taylor diagram for bias corrected daily temperature of three ESM outputs using three different methods, that is, BCCAQ (blue), QDM (red) and ISIMIP (purple) on annual and seasonal basis (MAM, DJA, SON and DJF). Distance between each model and the point labelled "observed" is a measure of how well each model reproduces reanalysis. The Pearson correlation coefficient indicates similarity in pattern between the bias corrected output with reanalysis data; the centred root mean square error (RMSE) is proportional to the distance from the point on the *x*-axis identified as "observed" (green contours); and the normalized standard deviations of the bias corrected model outputs is proportional to the radial distance from the origin (black contours) [Colour figure can be viewed at wileyonlinelibrary.com]

performed based on the bias corrected data using the best method, that is, QDM.

3.2 | Impact of SAI on mean temperature change

Figure 4a depicts plots of bias corrected future projections of mean temperature differences between the G4 and RCP4.5 scenarios over the Indonesian Maritime Continent, generated by three different models. The mean temperatures of G4 and RCP4.5 are not significantly different (*p*-value of Wilcoxon signed rank test is >0.05) in the early years of SAI deployment (2020–2025), consistent with global behaviour (Yu *et al.*, 2015) and expectations for the comparatively low total atmospheric burden of sulphate aerosols. In some years, BNU-ESM shows cooling over the Maritime Continent in G4 as compared with RCP4.5 by over 1.0°C. Conversely, MIROC-ESM

and MIROC-ESM-CHEM show substantially less cooling than BNU-ESM and in some years even show warmer temperatures than RCP4.5. After 2075, approximately 5 years after termination of geoengineering, the mean temperature in G4 scenarios increases sharply, consistent with previous findings on global mean (e.g., Ji *et al.*, 2018). For BNU-ESM, G4 was significantly cooler than RCP4.5. after 2075 (*p* < .05, Wilcoxon signed rank test), while the temperature difference between G4 and RCP4.5 generated by MIROC models were not significant.

Figure 4b shows the climate anomaly, that is, G4—historical of mean temperature. We observe a consistently increasing trend in mean temperatures, surpassing a 1°C change after 2050 for the MIROC models. The change under BNU-ESM model is consistently lower than MIROC models until 2069. Afterward, the anomaly in BNU-ESM is almost the same as for MIROC-ESM.

Figure 5a–c shows the spatial pattern of climate response to the G4. In line with the results in Figure 4,
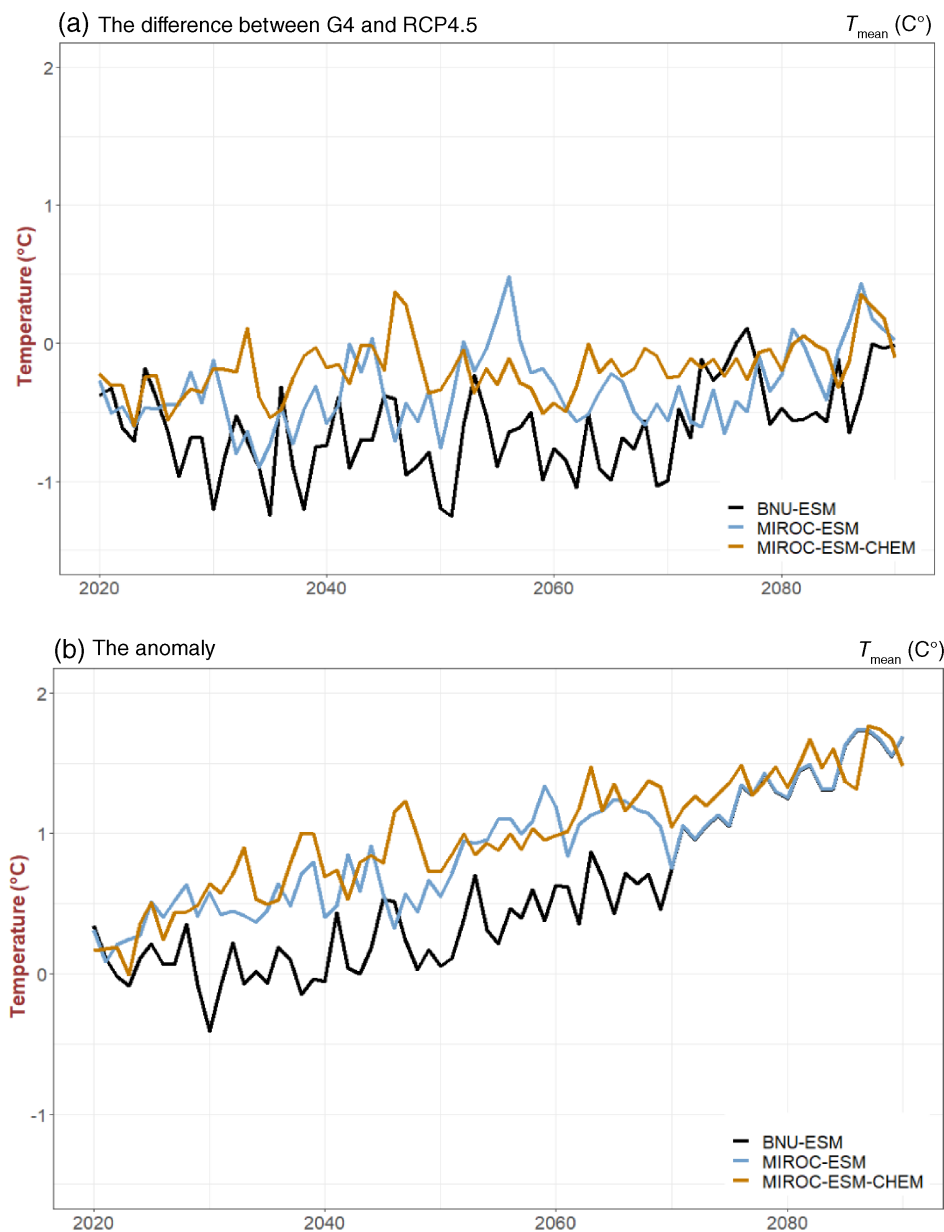
(a) The difference between G4 and RCP4.5 T_{mean} (C°)

(b) The anomaly T_{mean} (C°)

FIGURE 4 Plots of (a) annual mean temperature (ocean and land combined over Indonesian Maritime Continent) difference between G4 and RCP4.5, and (b) climate anomaly (G4-historical) [Colour figure can be viewed at wileyonlinelibrary.com]

we can see that the BNU-ESM model produces reduced mean temperatures relative to RCP4.5 over the whole region. Most regions show a statistically significant ($p < .05$) temperature reduction of 0.5°C–1°C. G4 gives lower temperatures than RCP4.5 over East Nusa Tenggara (NTT), Bali, and Papua, as well as the Indian ocean. We observe that the spatial response to the SAI application is more homogeneous under the BNU-ESM and MIROC-ESM models than the MIROC-ESM-CHEM model. MIROC-ESM shows only slight, but statistically significant ($p < .05$) temperature reductions with G4 as compared with RCP4.5 over the western part of Java (e.g., Jakarta), Jambi, southern part of Sumatra Island and South Kalimantan. MIROC-ESM-CHEM shows even lower temperature reductions under G4, which are often insignificant, as indicated by the greater stippled area.

Nevertheless, G4 tends to reduce the temperature of RCP4.5 over western Java and Kalimantan (with the exception of North Kalimantan).

Temperature changes after initiating SAI compared with the historical periods can be seen from the maps on Figure 5d–f. Under both MIROC models, the maps show that the mean temperature over most Indonesia region will be warmer within the periods of 2020–2069 compared with the historical periods. Nevertheless, negative difference between G4 and RCP4.5 as observed in Figure 5a–c confirmed that the mean temperature will be even warmer under RCP4.5. The BNU-ESM model shows a temperature anomaly of below 0.6°C (which is not significant over most land area), while under the MIROC models the temperature increase is projected to be 0.4°C–1°C above the level of historical periods. The three
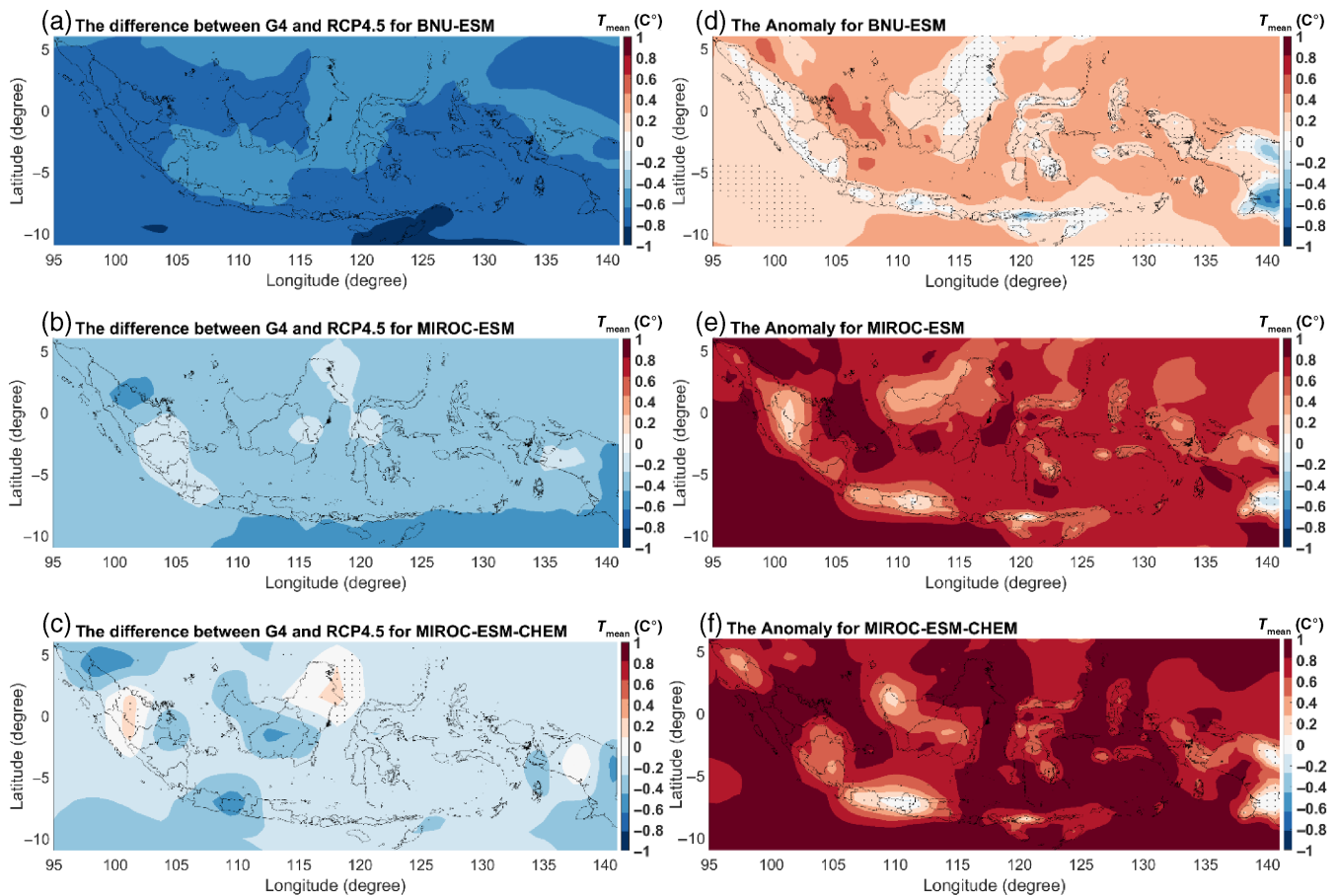
FIGURE 5 Spatial pattern of (a–c) mean temperature difference (G4-RCP4.5) over the 2020–2069 period and (d–f) climate anomalies: The mean temperature change with G4 deployment relative to the mean temperature averaged over the historical period of 1950–2005 (G4-historical) for BNU-ESM (top), MIROC-ESM (middle) and MIROC-ESM-CHEM (bottom). Stippling indicates grid points where differences or changes are not significant at the 5% level according to the Wilcoxon signed rank test [Colour figure can be viewed at wileyonlinelibrary.com]

models agree that the Java island, East Nusa Tenggara (NTT) and part of Papua would be the regions with the least warming under G4. Mean temperature changes over other regions vary across the different models. Under the G4 scenario, the temperature increase over Java will not exceed 0.3°C, which is lower than other regions.

The statistical test of exacerbation and moderation can be seen from Figure S7, illustrating how effective G4 is in offsetting climate change. Following Irvine *et al.* (2019), we define the effects of climate change as exacerbated if the absolute magnitude of the G4 anomaly from the historical is significantly greater than the RCP4.5 anomaly, and that they are moderated if G4 significantly reduces the absolute magnitude of the anomaly.

Under BNU-ESM and MIROC-ESM models, the map shows that SAI diminishes the effects of climate change over all Indonesia within the 2020–2069 period, and it is statistically significant except in parts of Papua. The BNU-ESM model clearly indicates that the difference

between anomaly under G4 and anomaly under RCP4.5 is greater over the sea reaching about 0.5°C–0.8°C. In the MIROC-ESM-CHEM model, the change of mean temperature is less homogenous than two other models, where the climate change is exacerbated in some areas and it is moderated over big islands such as Sumatra, Kalimantan, Sulawesi and Java islands.

3.3 | Impact of SAI on extreme temperature

Because the downscaling was performed for daily climate model output, we can assess changes in extreme temperature as well as mean temperature. SAI that reduces mean temperature will likely also be able to reduce the magnitude and intensity of extreme events such as extreme temperature (e.g., Curry *et al.*, 2014; Ji *et al.*, 2018). This section discusses the impact of G4 on the hottest day
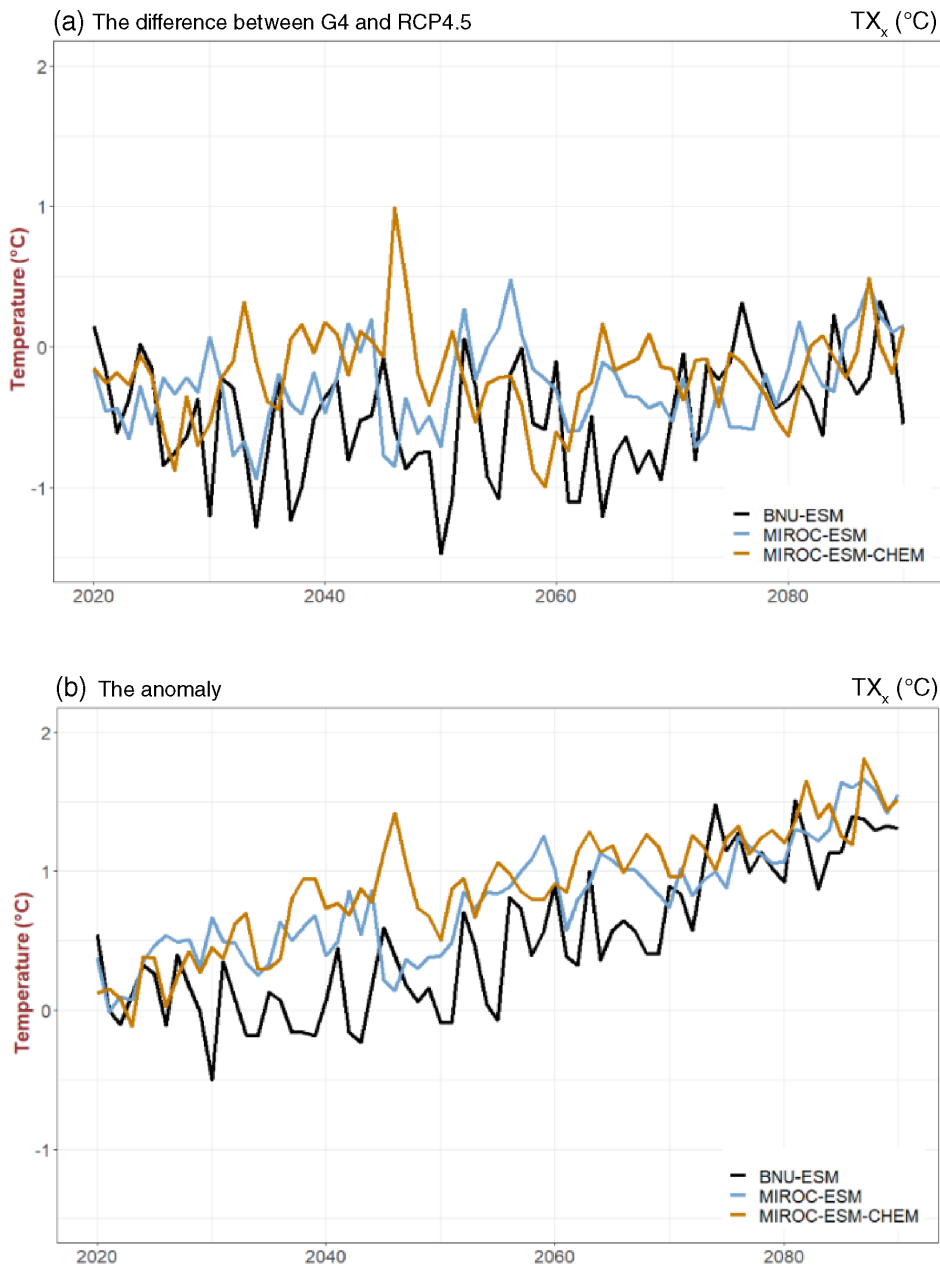
FIGURE 6 Plots of (a) maximum temperature (TX$_x$) difference between G4 and RCP4.5 averaged over land and sea of Indonesian Maritime Continent and (b) anomaly (G4-historical) [Colour figure can be viewed at wileyonlinelibrary.com]

(annual maximum value of daily maximum temperature; TX$_x$) in the Maritime Continent. Figure 6a shows plots of bias corrected future projection of TX$_x$ generated from the three different G4 simulations during the SAI application (2020–2069) period of and the post termination period (2070–2089). Each plot in Figure 6a provides information about the magnitude of TX$_x$ under G4 and RCP4.5, as well as mean of historical periods. We see that two G4 models (BNU-ESM and MIROC-ESM) consistently generate lower levels of TX$_x$ than RCP4.5 up to 2080, which includes a decade of termination. The G4 scenario effectively reduces TX$_x$ by about 0.6°C under BNU-ESM and 0.3°C under MIROC-ESM as compared with their respective RCP4.5 simulations. Meanwhile, MIROC-ESM-CHEM generates irregular patterns as to which years G4 decreases TX$_x$ as compared with RCP4.5. According to a Wilcoxon sign test, TX$_x$ differences between G4 and RCP4.5 in all models are statistically significant (p-value <.05).

Figure 6b indicates that the TX$_x$ anomaly tends to increase over time. Thus, the magnitude of TX$_x$ change relative to the historical period under G4 in the BNU-ESM model is again lower than the MIROC models within the period of SAI deployment. After 2070 the TX$_x$ anomaly for all models gradually increases with almost the same magnitude.

Previous studies conducted by Boer and Faqih (2004) as well as Hulme and Sheard (1999) found that there are
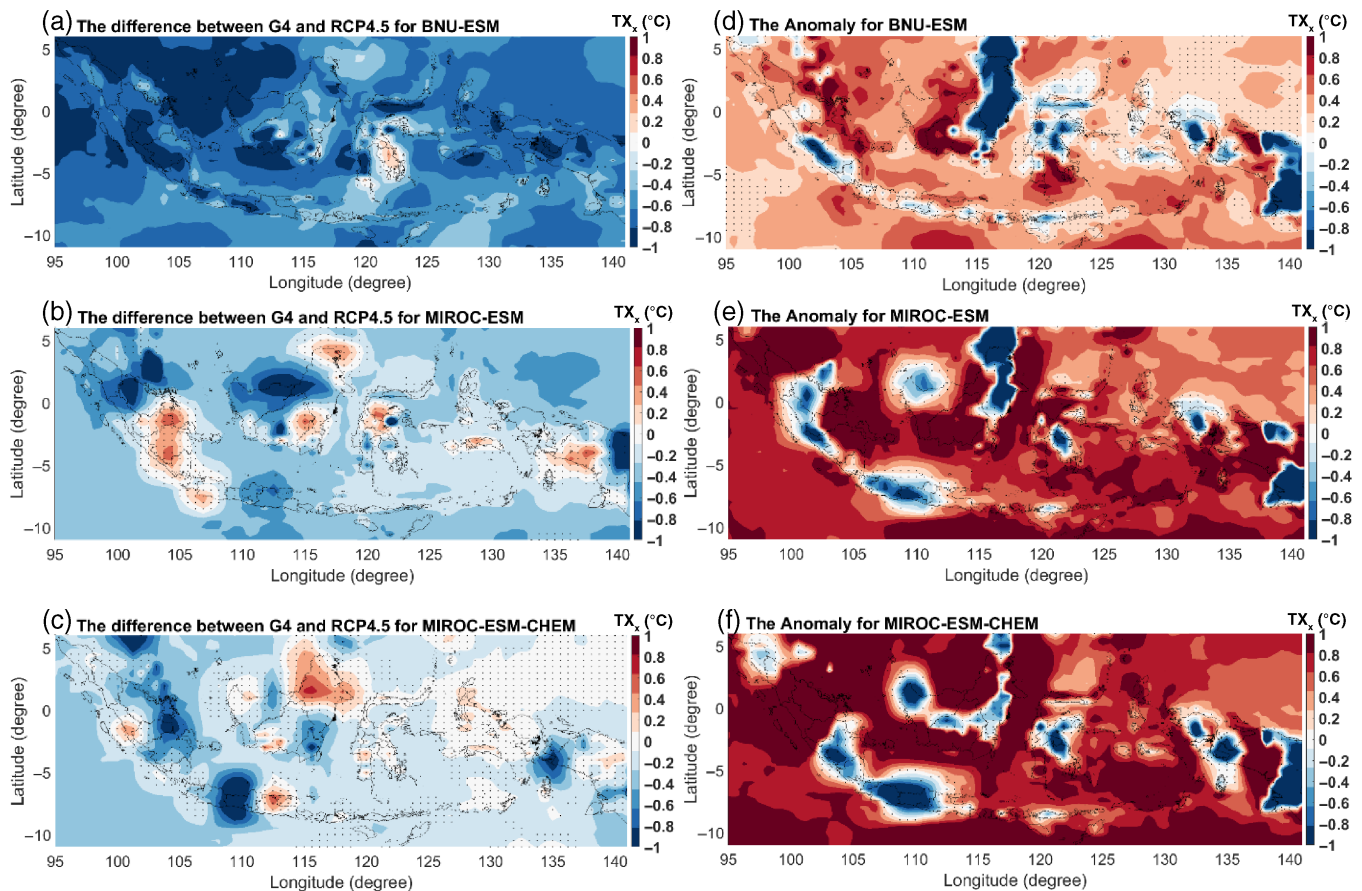
FIGURE 7   Spatial pattern of (a–c) maximum temperature (TX$_x$) difference (G4-RCP4.5) over the 2020–2069 period and (d–f) climate anomalies: The maximum temperature (TX$_x$) change with G4 deployment relative to the maximum temperature averaged over the historical period of 1950–2005 (G4-Historical) for BNU-ESM (top), MIROC-ESM (middle) and MIROC-ESM-CHEM (bottom). Stippling indicates grid points where differences or changes are not significant at the 5% level [Colour figure can be viewed at wileyonlinelibrary.com]

several different regimes of climate change response in Indonesia, depending on the location. The maps in Figure 7a–c demonstrate that the climate change impact on extreme temperature under G4 also varies. BNU-ESM shows that SAI will effectively reduce TX$_x$ in almost all regions by 0.1°C–1.5°C, with exceptions over Sulawesi and South Kalimantan where the impact is not statistically significant. It is interesting to note that the spatial variability of the impact is less homogenous over the southern part of Indonesia, which mostly falls in the anti-monsoonal region, following the definition of Aldrian and Susanto (2003). Moreover, the level of TX$_x$ reduction over the anti-monsoonal region is higher than over the monsoonal region. Meanwhile, MIROC-ESM indicates that SAI under G4 tends to result in an increase in TX$_x$ over several regions such as South Sumatra, West Java, South Sulawesi and Papua. However, the increase is not statistically significant. Most of Java island will experience significant increase in TX$_x$. MIROC-ESM-CHEM generates mostly insignificantly different in land except

over Central Java and Jambi where the TX$_x$ will significantly decrease.

Figure 7d–f show anomalies in TX$_x$ across the three models considered in this study. All models consistently show that under G4, TX$_x$ over Papua is significantly lower than in historical periods, with the level of reduction around 1°C. Similar patterns are observed at other places such as NTT, North Kalimantan, Southeast Sulawesi and Bengkulu (under BNU-ESM and MIROC-ESM models). Meanwhile TX$_x$ over most places in Indonesia increases in G4 by 0.1°C–1°C as compared with the historical period. Jambi, South Sumatra and South Kalimantan are places where the TX$_x$ is projected to warm significantly by around 1°C.

The test of exacerbation and moderation (Figure S8) indicates that climate changes are moderated over the sea, indicated by significant reduction on the absolute magnitude of the anomaly under G4; the anomaly over land areas is generally not statistically significant, meaning that the absolute magnitude of the anomaly under G4
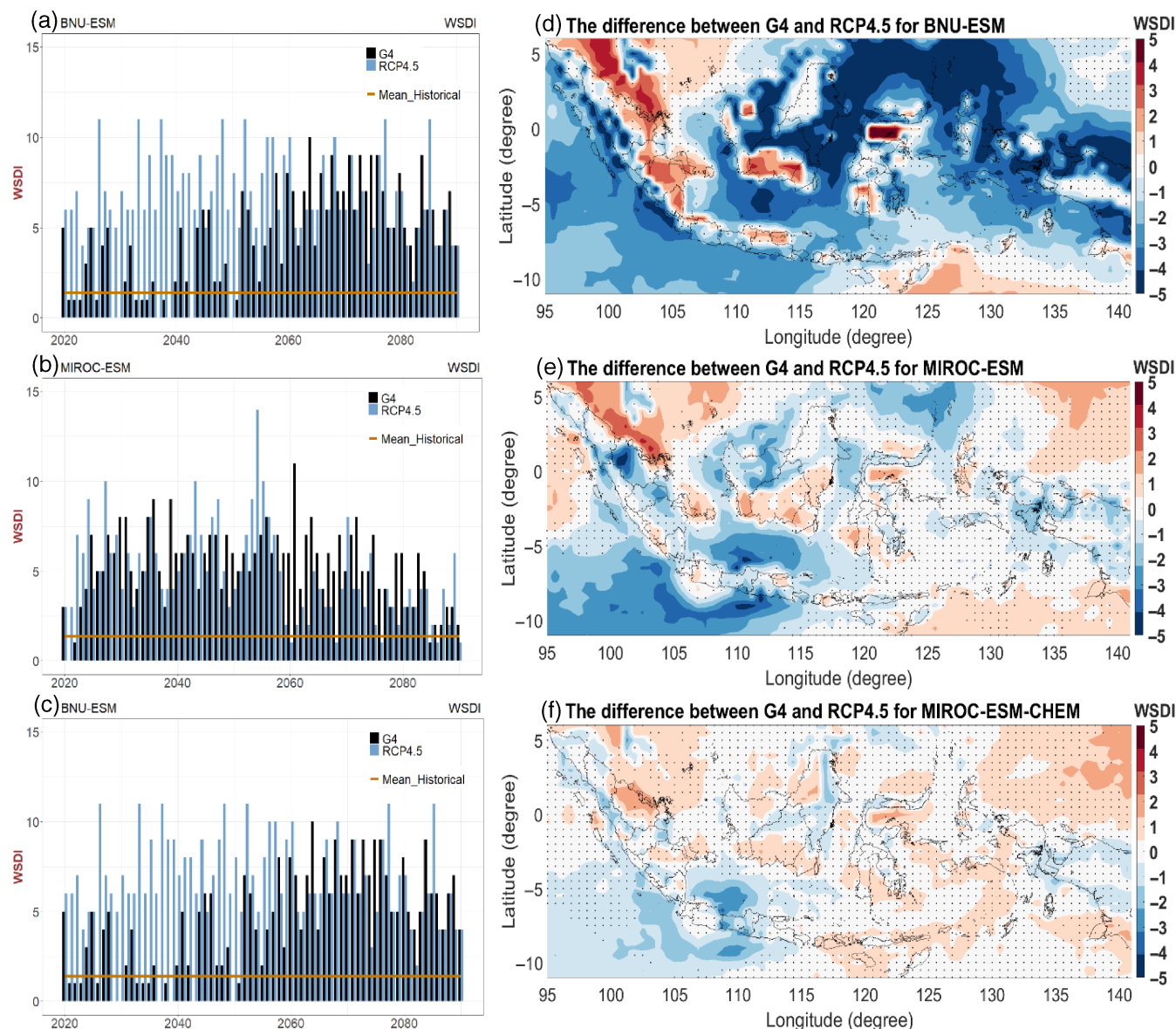
FIGURE 8 Time series of WSDI (days) under G4 and RCP4.5 in the periods of 2020–2089 with the historical level (mean of 1950–2005) shown as a black line for each ESM for BNU-ESM (a), MIROC-ESM (b) and MIROC-ESM-CHEM (c). Spatial pattern of WSDI difference between G4 and RCP4.5 for BNU-ESM (d), MIROC-ESM (e) and MIROC-ESM-CHEM (f). Stippling indicates grid points where differences or changes are not significant at the 5% level under the Wilcoxon signed rank test [Colour figure can be viewed at wileyonlinelibrary.com]

and under RCP4.5 is similar. It is interesting to note that with BNU-ESM, G4 exacerbates climate change over parts of Papua, North Kalimantan and South Sulawesi.

We now evaluate the impact of SAI on warm spell duration (WSDI), which is defined as the length of the longest streak of six or more days with the maximum temperature exceeding the 90th percentile of the baseline period. Figure 8 shows WSDI changes under the three different models.

From Figure 8a–c, we see that under BNU-ESM, G4 results in obviously reduced warm spell days compared with RCP4.5 over the period 2020–2069, ($p < .05$

according to a Wilcoxon test). After SAI termination (2070 onward), the WSDI in G4 rebounds to RCP4.5 values. Different results are observed for the MIROC models, where SAI is effective in reducing warm spell days only within a few years after SAI deployment, and gradually WSDI values rise to match the level of RCP4.5 and even surpass it after 2060. Both MIROC models have no significant differences between RCP4.5 and G4 for WSDI. The WSDI under SAI on post termination periods is about 1.3 days longer than under RCP4.5, which is statistically significant (p-value of Wilcoxon test equals .02). Under BNU-ESM model, the
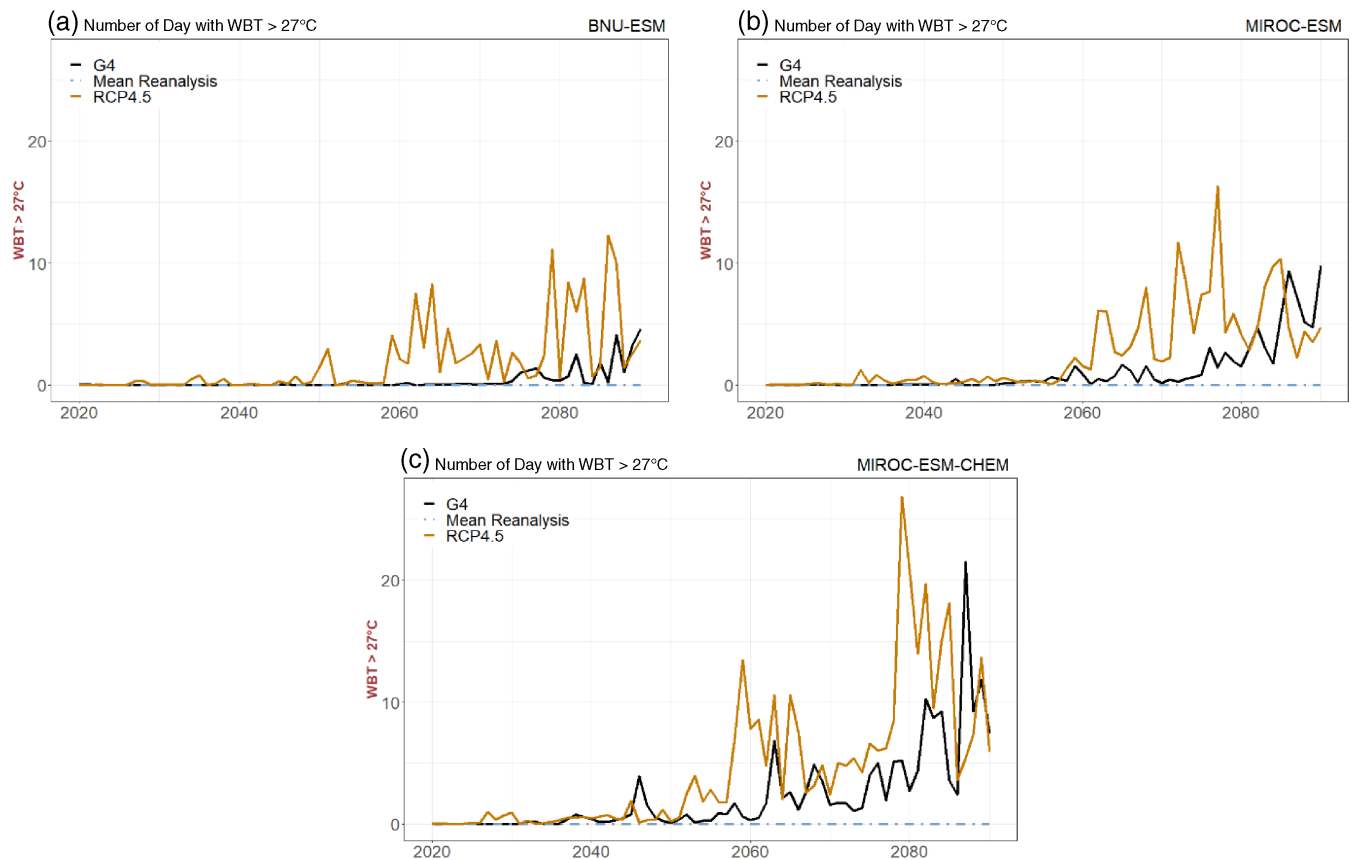
FIGURE 9 Plot of number of days per year with WBT > 27°C under three different models, that is, (a) BNU-ESM (b) MIROC-ESM (c) MIROC-ESM-CHEM, averaged over the 2,625 Indonesian grid for G4 (black), RCP4.5 (yellow), and the mean of reanalysis (green dashed line) [Colour figure can be viewed at wileyonlinelibrary.com]

warm spell days is simulated to be generally below the historical level up to 2050.

Figure 8d–f show spatial patterns of WSDI differences between G4 and RCP4.5. We see that, like the other indices examined in this study, the geographical response to SAI varies. Under BNU-ESM, the northern Java, southern Kalimantan and North Sumatra, Riau and Jambi experience longer warm spell days under SAI (about 1–3 days longer), while elsewhere WSDI is simulated to be 2–4 days shorter than under RCP4.5. The MIROC models generate similar patterns and a more homogeneous impact on WSDI with little significant change on land.

3.4 | Impact of SAI on relative humidity and wet bulb temperature

Relative humidity is important for livability such as human comfort, health and safety and is a major component of calculating WBT, which also depends on surface temperature and wind speed. WBT is the temperature of moist air, indicating the lowest temperature at which any fluid can be cooled through evaporation. Ideal relative

humidity is between 40% and 60% (Wolkoff, 2018). Indonesia's climate is the tropical Maritime Continental type, and one of the most humid regions in the world. Reanalysis data shows average relative humidity is about 70%–95%. Sumatra, Kalimantan, Sulawesi and Papua are regions with the highest humidity levels. Java island, Bali and NTT tend to be less humid, with the humidity level between 60% and 70%. However, west Java (including Jakarta) is the most humid place in Java. The three ESM projects relatively show small changes in mean humidity and WBT in future. MIROC-ESM and MIROC-ESM-CHEM show a slight increasing trend in relative humidity over the historical period for both RCP4.5 and G4. Under G4 within the period of 2020–2069, the relative humidity over land increases by 1%–5%. Java island, Bali and NTT experience increasing relative humidity, while the relative humidity over eastern part of Sumatra island and south Sumatra tends to be similar to the level of the historical period. The southern part of Papua experiences the highest relative humidity anomaly.

The average WBT over Indonesia based on reanalysis data and ESM outputs over the historical period was between 21°C and 25°C. This level is associated with
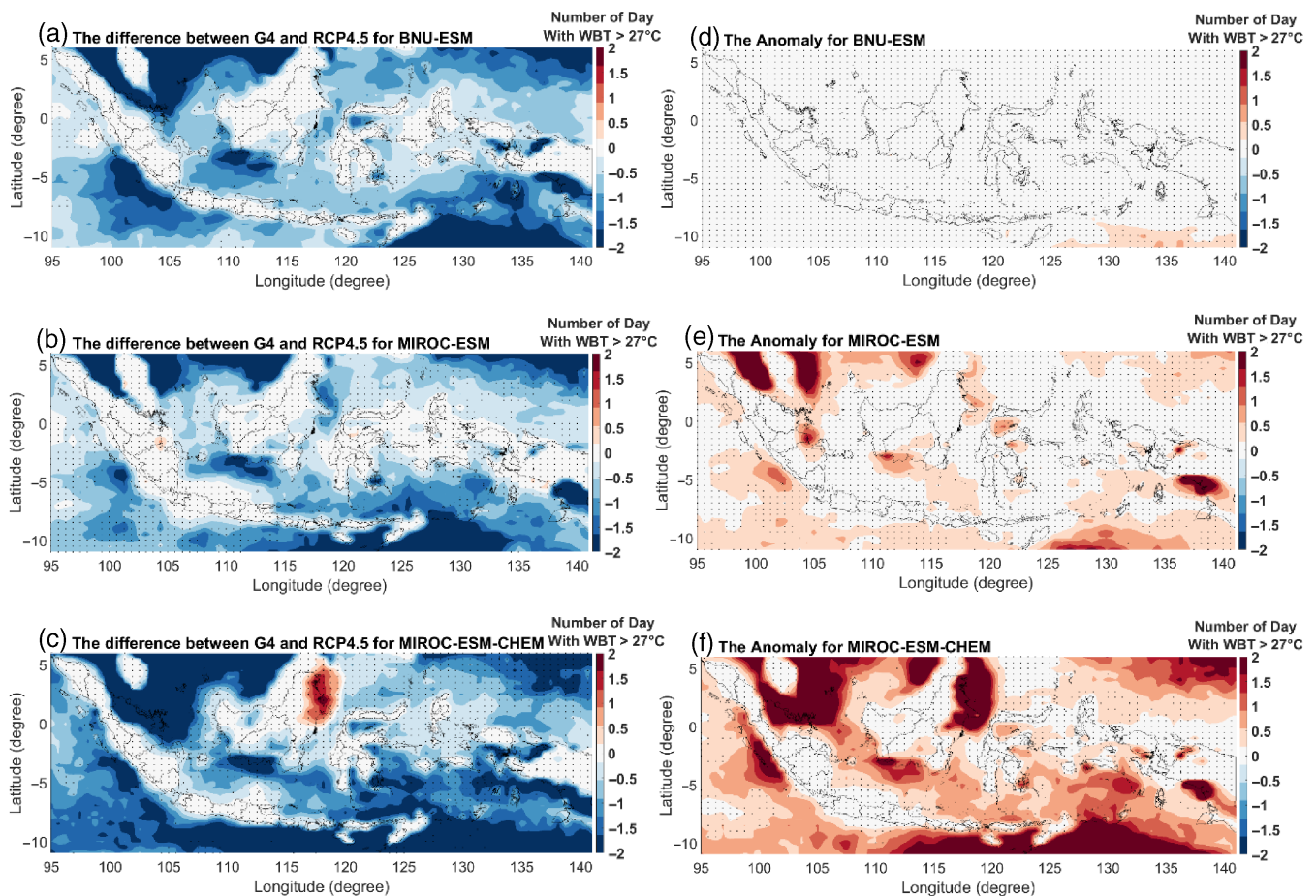
FIGURE 10 Number of days with WBT > 27°C differences between G4 and RCP4.5 under (a) BNU-ESM, (b) MIROC-ESM, (c) MIROC-ESM-CHEM and climate anomaly defined as difference between G4 and historical for (d) BNU-ESM, (e) MIROC-ESM, (f) MIROC-ESM-CHEM. Stippling indicates grid points where differences or changes are not significant at the 5% level under the Wilcoxon signed rank test (a–c), and under Wilcoxon rank sum test (d–f) [Colour figure can be viewed at wileyonlinelibrary.com]

medium risk of heat stress especially for heavy exercise or heavy work. However, changes in the average WBT are not as important as differences in the high end tail of the distribution. Here we focus on the future projection of annual number of days with the WBT > 27°C. This threshold is chosen due to its associated risk of heat related health problems and heat stress under conditions of intense and prolonged physical activity, especially for outdoor activities. Moreover, Sparke *et al.* (2001) and Caulfield *et al.* (2014) also defined that the WBT over 27°C is the "emergency" condition for livestock.

Figure 9 shows in the historical period the annual average number of days with WBT > 27°C of the historical periods is between 0 and 1. Hence it is a rare event. The occurrence of WBT > 27°C under RCP4.5 for all 3 models is projected to be higher than under the G4 scenario, with an increasing trend over the simulation. All models project that under SAI, the number of days with WBT > 27°C within the periods of 2020–2059 (i.e., 40 years since SAI deployment) would be below five events per year.

Consistent with the pattern observed on extreme temperature, the number of events will increase significantly after the termination of SAI. BNU-ESM exhibits lower likelihood of WBT > 27°C than the MIROC models. Under RCP4.5, the rate of extreme WBT days will be significantly higher than with SAI, and may be over 15 days per year. The spatial distribution of extreme WBT (Figure 10, left panel) confirms that compared with RCP4.5, all G4 models show reductions in number of days with WBT > 27°C up to 2 days in some locations especially over the ocean. However, over land the models indicate that SAI under G4 would not significantly reduce them relative to RCP4.5.

The maps in Figure 10d,f compare the change in the number of days with WBT > 27°C after SAI deployment compared with historical periods (G4-historical). We do not perform the exacerbation and moderation test as the average number of days with WBT > 27°C during historical period is close to zero, leading to similar results as Figure 10a–c. We observe no significant change in the number of events over different places in Indonesia for

the BNU-ESM model. The two MIROC models project that the number of days with WBT > 27°C would increase by about 1–2 days relative to historical period over several areas. North Kalimantan, North Sumatra (Medan), part of Papua and Timor sea are among places that will experience significant increase on the number of days with WBT > 27°C. We applied a Wilcoxon rank sum test to determine significance of change between the number of days with WBT > 27°C under G4 and historical level as the tested data are independent with different number of observation.

4 | DISCUSSION AND CONCLUSION

This article provides an overview of the impacts of SAI as represented by the G4 scenario on two relevant extreme temperature indices as well as mean temperature change for the Maritime Continent. Although our conclusion may be indicative of general effects of SAI, the specifics are based on the G4 experiment. The data we analysed was downscaled and bias corrected using QDM, which we found to be slightly better than BCCAQ and ISIMIP. Moreover, the impact of SAI on relative humidity and WBT have been investigated; to the best of our knowledge, the impact of SAI on WBT, for example, number of WBT > 27°C has never before been explored. Models indicate that the Maritime Continent exhibits considerable variability in the effects of climate change, particularly between the land and ocean parts. There are some consistent patterns to change, but also across-model differences, especially in the magnitude of the responses. Similarly, modelled changes in mean temperature and two extreme indices under SAI over the Maritime Continent also vary spatially. We note also that the spatial SAI impact on extremes is less uniform than mean temperature, and some regions do not show a substantial different in extreme temperature under SAI compared with under RCP4.5. However, all models agreed that SAI simulated cooler mean temperature than RCP4.5. While the climate change impact on mean temperature is exacerbated in some areas and it is moderated over big islands such as Sumatra, Kalimantan, Sulawesi and Java islands, the absolute magnitude of the anomaly over most of land areas under G4 and under RCP4.5 is about the same, with an exception that under BNU-ESM the climate change is exacerbated over part of Papua, North Kalimantan and South Sulawesi.

Our analysis indicates that SAI will tend to decrease the mean temperature over Papua and NTT relative to the 1950–2005 mean. The mean temperature in other places would remain at or close to its historical level

under G4. Nevertheless, the warming occurs under SAI is lower than without SAI. It should also be noted that the G4 experiment was not designed to maintain temperatures at a prescribed level (e.g., the 1950–2005 level), but to determine the impact of a constant SO_2 aerosol injection load as greenhouse gas concentrations increase according to RCP4.5. Hence the near balance in temperatures over the Maritime Continent is an unintended effect. We would expect the G4 experiment to provide insights on spatial patterns of variability and degree of confidence in ensemble predictions. The daily maximum temperature extreme measured by TX_x over Papua and NTT (also northern Kalimantan, southeast Sulawesi and Bengkulu) is simulated to be substantially reduced under G4 relative to RCP4.5, while elsewhere it increases slightly by 0.3°C–0.5°C. G4 would shorten the warm spell duration (WSDI) over those particular regions (Papua, NTT, northern Kalimantan, Southeast Sulawesi and Bengkulu) by 1–2 days, especially during the early period of SAI deployment.

Climate change has impacted Indonesia by increasing its vulnerability to weather-related disasters such as forest fires and drought. The National Agency for Disaster Management (BNPB) reported that Riau, Jambi, South Sumatra, western, southern and central Kalimantan are high risk regions from fire. These regions are mainly covered by forest and fires have been consistent occurrences over the last decade whether set by human or by weather. The total forest lost in 2019 was about 857,000 Ha. East Nusa Tenggara (NTT) and Papua are two regions with high risk of drought. High temperatures tend to exacerbate drought conditions and increase the likelihood of fires. Under SAI, the temperature in those particular regions is projected to be cooler. Moreover, Sen (2015) pointed out that dry spells may describe periods of precipitation deficits resulting in occasional water shortages, droughts and arid conditions. A projected shortening of WSDI under SAI may be useful for reducing some of the dangers of dry spells.

We note that the variability of SAI impacts is higher over southern Indonesia, which is mostly in the monsoonal region (Aldrian and Susanto, 2003). Yamanaka (2016) argued that warming of the southern region of Indonesia is due to a combination of factors, such as exacerbation of heat extremes by drying, as well as changes in the El Niño Southern Oscillation (ENSO). Detailed statistical analysis of ENSO changes under solar geoengineering (Gabriel and Robock, 2015; Guo et al., 2018) found no significant change in variability. In general SRM acts to counter the general greenhouse gas trends of wet becoming wetter and dry becoming drier (Tilmes et al., 2013; Ji et al., 2018), but the intertropical convergence zone may be an exception to this. The equatorial edge of the Hadley cell shows smaller

seasonal amplitude of latitudinal movement under solar geoengineering (Smyth *et al.*, 2017; Guo *et al.*, 2018), and hence would be expected to influence Indonesia. Wang *et al.* (2018) note that the tropical cyclone season is moved about a month earlier under G4 than RCP4.5, a consistent response across ESM and cyclone basins, and which could be related to the reduced heating under SRM and reduced amplitude of ITCZ motion. Given the importance of deep convention systems in the region, the changes near the tropopause noted under SRM by Pitari *et al.* (2014) and Wang *et al.* (2018) would be very significant to wet and dry seasons in the Maritime Continent. The response at the 100 hPa level appears to be model-dependent and resumably strongly affected by the details of aerosol parameterization and physics employed by the SRM. Although it is beyond the scope of the present work to thoroughly investigate these factors, they are important for understanding how temperatures in Indonesia may change under climate change.

We see that changes in mean temperature and TX_x in two models (e.g., BNU ESM and MIROC-ESM) are quite consistent in terms of their spatial pattern, although the magnitude of the change is different. Meanwhile, the spatial impacts of MIROC-ESM-CHEM differs significantly from those two models. However, we can expect that SAI would be effective at reducing mean temperature and the magnitude of extremes, consistent with the global trend as found by Jones *et al.* (2018). All models consistently show that under GeoMIP experiment G4, the mean temperature rises over Indonesia could be kept within 0.5°C– 1°C, that is, below the Paris Agreement (global) target. Moreover, during post termination periods, models show that the temperature level would rebound to RCP4.5 but would never rise higher than under RCP4.5.

We also investigated the number of days with WBT > 27°C. The choice of 27°C as the threshold refers to previous studies indicating that this represents an exposure to heat stress leading to exacerbated health risk (mental fatigue, physical depletion, dehydration, etc.). A study by the Sports Medicine and Physical Fitness Committee of the American Academy of Paediatrics (2000) defined WBT over 27°C as a high risk condition indicating discontinuation of physical activity for nonacclimated persons or persons with pre-existing health conditions. Furthermore, WBT > 29°C is categorized as an extreme risk which may lead to body collapse and death.

Discussion on the SAI impact to relative humidity and heat stress in Indonesia is an important issue, which may induce heat-related health risk and mortality especially in a fast growing city such as Jakarta. Varquez *et al.* (2020) focused their study on the future changes in heat-related mortality of elderly citizen in Jakarta and found that heat-related mortality of the elderly in Jakarta

would increase in the 2050s because of population growth and climate change. Moreover, they found that mitigating climate change by following the RCP 2.6 greenhouse gas emissions scenario could reduce the August elderly mortality count by 17%. Our research examined the G4 scenario which follows the RCP4.5 pathways and does not directly equate to RCP2.6, but Varquez *et al.* (2020) may be a useful guide to estimating elderly mortality under G4 scenario.

All models indicated the impact of SAI on relative humidity change would be heterogeneous over Indonesia. Java, Bali and NTT would become more humid under SAI compared with average humidity level during the historical periods. Nevertheless, the models project that SAI would effectively reduce the humidity level of RCP4.5 over west Java (including Jakarta). The average number of days with WBT > 27°C would increase significantly during the SAI deployment compared with historical levels, but much less than under RCP4.5, and events will significantly increase in the post-termination periods.

Coffel *et al.* (2019) highlighted the link between extreme temperature and humid-heat change in the context of land-surface drying. The study found that for many places global warming lowers soil moisture, reducing relative humidity level and heat stress, thus providing a negative feedback on WBT. The drying associated with warming dampens mid-latitude WBT increases by up to 0.5°C, and also dampens the rise in frequency of dangerous humid-heat (WBT > 27°C) in parts of North America and Europe. In our study we find that changes by SAI in WBT extremes are larger over the oceans than land. This is therefore less likely to have impacts on health and mortality than if changes were greater over land. This result tends to contradict intuitive understanding of SRM impacts which results in a lower global humidity and fewer floods, but the Maritime Continent is somewhat different form this global picture in having reduced (precipitation–evaporation) and runoff under RCP4.5 than G4 (Wei *et al.*, 2018). This results in smaller changes in WBT over the land regions than oceans for Indonesia, and suggests that for WBT, G4 may not be analogous to RCP2.6, despite similar expected impacts in surface temperatures. The simulation of WBT would be better done by high resolution dynamic models than the downscaling methods that we used, but this preliminary research emphasizes that differences in complex climate impacts require sophisticated impact models.

Overall, we conclude that SAI could reduce some of the negative impacts of climate change induced by temperature. Since drought is tied to temperature extremes (along with precipitation and other climate variables), SAI could be effective at reducing the risk of drought in highly vulnerable areas. TX_x over the fire spots will be projected to be higher than in the historical period, and

so simulations with high resolution dynamic models under SAI may be an important area of future research. Ours is the first study of detailed, high resolution projections of the effects of SAI on Indonesia and the Maritime Continent, and provides much needed information for policy makers. Moreover, this study provides understanding of the general characteristics (pattern and magnitude) of future climate change hazards under SAI in Indonesia, setting the foundation for further analysis of impacts to development sectors. Further application is in the process of developing the National Roadmap of mitigation and adaptation strategies to future climate change impact, especially dealing with the unique characteristics of each region, with regard to fire and drought risk reduction. Moreover, the analysis of relative humidity and WBT are relevant for strategic planning in the health sector.

Although this study found many interesting results about the impact of SAI on temperatures in the Indonesian Maritime Continent, we did not evaluate overall drivers of the climate system over the Indonesian Maritime Continent. This would make a useful topic of future research. Moreover, although the maps provide some geographic information, all aggregate metrics in this study were calculated over the combined sea and land areas, which can introduce a certain degree of bias. Because climate impacts could be substantially different between land and sea, future research can also be directed to analyse the SAI impacts separately between land and sea.

DATA AVAILABILITY STATEMENT

MERRA-2 output is available via MDISC, managed by the NASA Goddard Earth Sciences (GES) Data and Information Services Center (DISC). All climate model output used here is available via the Earth System Grid Federation (ESGF).

ORCID

Heri Kuswanto https://orcid.org/0000-0003-0300-7286

REFERENCES

ADB. (2019) *Asian Development Outlook 2019: strengthening disaster resilience*. Philipina: Asian Development Bank.

Aldrian, E. and Susanto, R.D. (2003) Identification of three dominant rainfall regions within Indonesia and their relationship to sea surface temperature. *International Journal of Climatology*, 23(12), 1435–1452.

Budyko, M.I. (1977) Present-day climatic changes. *Tellus*, 29(3), 193–204.

Badan Nasional Penanggulangan Bencana (BNPB). (2019) *Indeks Resiko Bencana Indonesia Tahun 2019*. Indonesia: Direktorat Pengurangan Risiko Bencana Badan Nasional Penanggulangan Bencana.

Boer, M., and Faqih, M. (2004) Global climate forcing factor and rainfall variability in West Java: case study in Bandung district. *Agromet*, 18(2), 1–12.

Cannon, A.J., Hiebert, J., Werner, A., Sobie, S. and Hiebert, M.J. (2016) *ClimDown: Climate Downscaling Library for Daily Climate Model Output*. Pacific Climate Impacts Consortium (PCIC): Victoria, BC, Canada.

Cannon, A.J., Sobie, S.R. and Murdock, T.Q. (2015) Bias correction of GCM precipitation by quantile mapping: how well do methods preserve changes in quantiles and extremes? *Journal of Climate*, 28(17), 6938–6959.

Caulfield, M.P., Cambridge, H., Foster, S.F. and McGreevy, P.D. (2014) Heat stress: a major contributor to poor animal welfare associated with long-haul live export voyages. *The Veterinary Journal*, 199(2), 223–228.

Chen, Y., Liu, A. and Moore, J.C. (2020) Mitigation of Arctic permafrost carbon loss through stratospheric aerosol geoengineering. *Nature Communications*, 11(2430), 1–10.

Coffel, E.D., Horton, R.M., Winter, J.M. and Mankin, J.S. (2019) Nonlinear increases in extreme temperatures paradoxically dampen increases in extreme humid-heat. *Environmental Research Letters*, 14(8), 1–10.

Crutzen, P. (2006) Albedo enhancements by stratospheric sulfur injections: a contribution to resolve a policy dilemma. *Climatic Change*, 77, 211–220.

Curry, C.L., Sillmann, J., Bronaugh, D., Alterskjaer, K., Cole, J.N.S., Ji, D., Kravitz, B., Kristjánsson, J.E., Moore, J.C., Muri, H., Niemeier, U., Robock, A., Tilmes, S. and Yang, S. (2014) A multimodel examination of climate extremes in an idealized geoengineering experiment. *Journal of Geophysical Research: Atmospheres*, 119, 3900–3923.

Da-Allada, C.Y., Baloïtcha, E., Alamou, E.A., Awo, F.M., Bonou, F., Pomalegni, Y., Biao, E.I., Obada, E., Zandagba, J.E., Tilmes, S. and Irvine, P.J. (2020) Changes in west African summer monsoon precipitation under stratospheric aerosol geoengineering. *Earth's Future*, 8, 1–13.

Dagon, K. and Schrag, D.P. (2016) Exploring the effects of solar radiation management on water cycling in a coupled land–atmosphere model. *Journal of Climate*, 29(7), 2635–2650.

Effiong, U. and Neitzel, R.L. (2016) Assessing the direct occupational and public health impacts of solar radiation management with stratospheric aerosols. *Environmental Health*, 15(7), 1–9.

Faqih, A., Hidayat, R., Jatmiko, S.D. and Radini, D. (2016) Climate modeling and analysis for Indonesia 3rd national communication (TNC): Historical and climate and future climate scenarios in Indonesia. Final Report. Ministry of Environment and Forestry (MoEF). United National Development Programme (UNDP) and Bogor Agicultural University.

Fernades, K., Verchot, L., Baethgen, W., Velez, V.G., Vasquez, M.P. and Martius, C. (2017) Heightened fire probability in Indonesia in non-drought conditions: the effect of increasing temperatures. *Environmental Research Letters*, 12(5), 1–11.

Gabriel, C.J. and Robock, A. (2015) Stratospheric geoengineering impacts on El Niño/southern oscillation. *Atmospheric Chemistry and Physics*, 15, 11949–11966.

Govindasamy, B. and Caldeira, K. (2000) Geoengineering earth's radiation balance to mitigate CO2-induced climate change. *Geophysical Research Letters*, 27, 2141–2144.

Gudmundsson, L., Bremnes, J.B., Haugen, J.E. and Engen-Skaugen, T. (2012) Technical note: downscaling RCM precipitation to the station scale using statistical transformations: a comparison of methods. *Hydrology and Earth System Sciences*, 16(9), 3383–3390.

Guo, A., Moore, J.C. and Ji, D. (2018) Tropical atmospheric circulation response to the G1 sunshade geoengineering radiative forcing experiment. *Atmospheric Chemistry and Physics*, 18(13), 8689–8706.

Harding, A.R., Ricke, K., Heyen, D., MacMartin, D.G. and Cruz, J.M. (2020) Climate econometric models indicate solar geoengineering would reduce inter-country income inequality. *Nature Communications*, 11(227), 227.

Hempel, S., Frieler, K., Waraszawski, L., Schewe, J. and Piontek, F. (2013) A trend-preserving bias correction: the ISI-MIP approach. *Earth System Dynamics*, 4, 219–236.

Heo, J.-H., Ahn, H., Shin, J.-Y., Kjeldsen, T.R. and Jeong, C. (2019) Probability distributions for a quantile mapping technique for a bias correction of precipitation data: a case study to precipitation data under climate change. *Water*, 11(7), 1–20.

Hidalgo, H.G., Dettinger, M.D. and Cayan, D.R. (2008) *Downscaling with Constructed Analogues: Daily Precipitation and Temperature Fields over the United States, CEC-500-2007-123*. USA: California Energy Commission.

Hulme, M. and Sheard, N. (1999) *Climate Change Scenarios for Indonesia*. Norwich, UK: Climatic Research Unit.

Hunter, R.D. and Meentemeyer, R.K. (2005) Climatologically aided mapping of daily precipitation and temperature. *Journal of Applied Meteorology*, 44, 1501–1510.

IPCC. (2014) *Climate Change 2014: Synthesis Report. Contribution of Working Groups I, II and III to the Fifth Assessment Report of the Intergovernmental Panel on Climate Change [Core Writing Team, R.K. Pachauri and L.A. Meyer (eds.)]*. Geneva, Switzerland: IPCC.

Irvine, P.J., Kravitz, B., Lawrence, M., Gerten, D., Hendy, E., Caminade, C., Gosling, S.N., Hendy, E.J., Kassie, B.T., Kissling, W.D., Muri, H., Oschlies, A. and Smith, S. (2017) Towards a comprehensive climate impacts assessment ofsolar geoengineering. *Earth's Future*, 5(1), 93–106.

Irvine, P.J., Emanuel, K., He, J., Horowitz, L.W., Vecchi, G. and Keith, D. (2019) Halving warming with idealized solar geoengineering moderates key climate hazards. *Nature Climate Change*, 9, 295–299.

Ji, D., Wang, L., Feng, J., Wu, Q., Cheng, H., Zhang, Q., Yang, J., Dong, W., Dai, Y., Gong, D., Zhang, R.-H., Wang, X., Liu, J., Moore, J.C., Chen, D. and Zhou, M. (2014) Description and basic evaluation of Beijing Normal University Earth System Model (BNU-ESM) version 1. *Geoscientific Model Development*, 7, 2039–2064.

Ji, D., Fang, S., Curry, C.L., Kashimura, H., Watanabe, S., Cole, J.N.S., Lenton, A., Muri, H., Kravitz, B. and More, J.C. (2018) Extreme temperature and precipitation response to solar dimming and stratospheric aerosol geoengineering. *Atmospheric Chemistry and Physics Discussions*, 18, 10133–10156.

Jones, A.C., Hawcroft, M.K., Haywood, J.M., Jones, A., Guo, X. and Moore, J.C. (2018) Regional climate impacts of stabilizing global warming at 1.5 K using solar geoengineering. *Earth's Future*, 6(2), 230–251.

Karami, K., Tilmes, S., Muri, H. and Mousavi, S.V. (2020) Storm track changes in the middle east and North Africa under stratospheric aerosol geoengineering. *Geophysical Research Letters*, 47(14), 1–9.

Kravitz, B., MacMartin, D.G., Robock, A., Rasch, P.J., Ricke, K.L., Cole, J.N.S., Curry, C.L., Irvine, P.J., Ji, D. and Keith, D.W. (2014) A multi-model assessment of regional climate disparities caused by solar geoengineering. *Environmental Research Letters*, 9(7), 1–7.

Kravitz, B., Robock, A., Boucher, O., Schmidt, H., Taylor, K.E., Stenchikov, G. and Schulz, M. (2011) The geoengineering model intercomparison project (GeoMIP). *Atmospheric Science Letters*, 12, 162–167.

Lanzante, J.R., Adams-Smith, D., Dixon, K.W., Nath, M. and Whitlock, C.E. (2019) Evaluation of some distributional downscaling methods asapplied to daily maximum temperature with emphasis on extremes. *International Journal of Climatology*, 40(3), 1571–1585.

Maurer, E.P., Hidalgo, H.G., Das, T., Dettinger, M.D. and Cayan, D.R. (2010) The utility of daily 10 large-scale climate data in the assessment of climate change impacts on daily streamflow in California. *Hydrology and Earth System Sciences*, 14, 1125–1138.

Measey, M. (2010) Indonesia: a vulnerable country in the face of climate change. *Global Majority E-Journal*, 1(1), 31–45.

Meinshausen, M., Smith, S.J., Daniel, J.S., Kainuma, M.L.T., Lamarque, J.-F., Matsumoto, K., Montzka, S.A., Raper, S.C.B., Riahi, K., Thomson, A., Velders, G.J.M. and van Vuuren, D.P.P. (2011) The RCP greenhouse gas concentrations and their extensions from 1765 to 2300. *Climatic Change*, 109, 213–241.

Moore, J.C., Yue, C., Zhao, L., Guo, X., Watanabe, S. and Ji, D. (2019) Greenland ice sheet response to stratospheric aerosol injection geoengineering. *Earth's Future*, 7(2), 1451–1463.

Moore, J.C., Jevrejeva, S. and Grinsted, A. (2010) Efficacy of geoengineering to limit 21st century sea-level rise. *Proceedings of the National Academy of Sciences*, 107(36), 15699–15703.

National Research Council. (2015) *Climate Intervention: Reflecting Sunlight to Cool Earth*. Washington, DC: The National Academies Press.

Parkhurst, H., Nurdiati, S. and Sopaheluwakan, A. (2019) Analysis of drought characteristics in southern Indonesia based on return period measurement. In: The 5th International Seminar on Sciences IOP Conference Series: Earth and Environmental Science, p. 299.

Panofsky, H.A., and Brier, G.W. (1968) *Some Applications of Statistics to Meteorology*. University park, PA, USA: The Pennsylvania State University. pp. 224.

Piani, C., Haerter, J.O. and Coppola, E. (2010) Statistical bias correction for daily precipitation in regional climate models over Europe. *Theoretical and Applied Climatology*, 99, 187–192.

Pinto, I., Jack, C., Lennard, C., Tilmes, S. and Odoulami, R.C. (2020) Africa's climate response to solar radiation management with stratospheric aerosol. *Geophyical Research Letters*, 47(2), 1–10.

Pitari, G., Aquila, V., Kravitz, B., Robock, A., Watanabe, S., Cionni, I., Luca, N.D., Genova, G.D., Mancini, E. and Tilmes, S. (2014) Stratospheric ozone response to sulfate geoengineering: results from the geoengineering model intercomparison project (GeoMIP). *Journal of Geophysical Research – Atmospheres*, 119(2), 2629–2653.

Pongratz, J., Lobell, D.B., Cao, L. and Caldeira, K. (2012) Crop yields in a geoengineered climate. *Nature Climate Change*, 2(2), 101–105.

Proctor, J., Hsiang, S., Burney, J., Burke, M. and Schlenker, W. (2018) Estimating global agricultural effects of geoengineering using volcanic eruptions. *Nature*, 560, 480–483.

Rahman, A.A., Artaxo, P., Asrat, A. and Parker, A. (2018) Developing countries must lead on solar geoengineering research. *Nature*, 556, 22–24.

Ricke, K.L., Morgan, M.G. and Allen, M.R. (2010) Regional climate response to solar radiation management. *Nature Geoscience*, 3, 537–541.

Rienecker, M., Suarez, M., Gelaro, R., Todling, R., Bacmeister, J., Liu, E., Bosilovich, M., Schubert, S., Takacs, L., Kim, G.-K., Bloom, S., Chen, J., Collins, D., Conaty, A., Da Silva, A., Gu, W., Joiner, J., Koster, R., Lucchesi, R. and Woollen, J. (2011) MERRA-NASA's modern-era retrospective analysis for research and applications. *Journal of Climate*, 24, 3624–3648.

Sarmini, E. and Faqih, A. (2016) Extreme climate events and their impacts on food crop in Indonesia. *Jurnal Sumberdaya Lahan*, 10(2), 115–128.

Sarr, M.A., Seidou, O., Tramblay, Y. and Aldouni, S.E. (2015) Comparison of downscaling methods for mean and extreme precipitation in Senegal. *Journal of Hydrology: Regional Studies*, 4, 369–385.

Sen, Z. (2015) *Applied Drought Modeling, Prediction, and Mitigation*. Netherland: Elsevier.

Smyth, J.E., Russotto, R.D. and Storelvmo, T. (2017) Thermodynamic and dynamic responses of the hydrological cycle to solar dimming. *Atmospheric Chemistry and Physics*, 17, 6439–6453.

Sparke, E.J., Young, B.A., Gaughan, J.B., Holt, M. and Goodwin, P.J. (2001) *Heat Load in Feedlot Cattle*. North Sydney, NSW, Australia: Meat and Livestock Australia.

Sunyer, M., Madsen, H. and Ang, P. (2012) A comparison of differentregional climate models and statistical downscaling methods forextreme rainfall estimation under climate change. *Atmospheric Research*, 103, 119–128.

Supari, T., Tangang, F., Juneng, L. and Aldrian, E. (2017) Observed changes in extreme temperature and precipitation over Indonesia. *International Journal of Climatology*, 37(4), 1979–1997.

Switanek, M.B., Troch, P.A., Castro, C.L., Leuprecht, A., Chang, H.-I., Mukherjee, R. and Demaria, E.M.C. (2017) Scaled distribution mapping: a bias correction method that preserves raw climate model projected changes. *Hydrology and Earth System Sciences*, 21(6), 2649–2666.

Tang, J., Niu, X., Wang, S., Gao, H., Wang, X. and Wu, J. (2016) Statistical downscaling and dynamical downscaling of regional climate in China: present climate evaluations and future climate projections. *Journal of Geophysical Research – Atmospheres*, 121(2), 2110–2129.

Taylor, K.E., Stouffer, R.J. and Meehl, G.A. (2012) An overview of CMIP5 and the experiment design. *Bulletin of the American Meteorological Society*, 93, 485–498.

Teutschbein, C. and Seibert, J. (2012) Bias correction of regional climatemodel simulations for hydrological climate-change impact studies: review and evaluation of different methods. *Journal of Hydrology*, 456-457, 12–29.

Tilmes, S., Fasullo, J., Lamarque, J.F., Marsh, D.R., Mills, M., Alterskjaer, K., Muri, H., Kristjánsson, J.E., Boucher, O., Schulz, M., Cole, J.N.S., Curry, C.L., Jones, A., Haywood, J., Irvine, P.J., Ji, D., Moore, J.C., Karam, D.B., Kravitz, B., Rasch, P.J., Singh, B., Yoon, J.H., Niemeier, U., Schmidt, H., Robock, A., Yang, S. and Watanabe, S. (2013) The hydrological impact of geoengineering in the geoengineering model intercomparison project (GeoMIP). *Journal of Geophysical Research: Atmospheres*, 118, 11036–11058.

Trisos, C.H., Amatulli, G., Gurevitch, J., Robock, A., Xia, L. and Zambri, B. (2018) Potentially dangerous consequences for biodiversity of solar geoengineering implementation and termination. *Nature Ecology & Evolution*, 2, 475–482.

Trzaska, S. and Schnarr, E. (2014) A Review of Downscaling Methods for Climate Change Projections. African and Latin American Resilience to Climate Change (ARCC). United States Agency for International Development by Tetra Tech ARD.

Varquez, A.C.G., Darmanto, N.S., Honda, Y., Ihara, T. and Kanda, M. (2020) Future increase in elderly heat related mortality of a rapidly growing Asian megacity. *Scientific Reports*, 10, 9304.

Wang, Q., Moore, J.C. and Ji, D. (2018) A statistical examination of the effects of stratospheric sulfate geoengineering on tropical storm genesis. *Atmospheric Chemistry and Physics*, 18, 9173–9188.

Watanabe, S., Miura, H., Sekiguchi, M., Nagashima, T., Sudo, K., Emori, S. and Kawamiya, M. (2008) Development of an atmospheric general circulation model for integrated earth system modeling on the earth simulator. *Journal of the Earth Simulator*, 9, 27–35.

Watanabe, S., Hajima, T., Sudo, K., Nagashima, T., Takemura, T., Okajima, H., Nozawa, T., Kawase, H., Abe, M., Yokohata, T., Ise, T., Sato, H., Kato, E., Takata, K., Emori, S. and Kawamiya, M. (2011) MIROC-ESM 2010: model description and basic results of CMIP5-20c3m experiments. *Geoscientific Model Development*, 4, 845–872. https://doi.org/10.5194/gmd-4-845-2011.

Wei, L., Ji, D., Miao, C., Muri, H. and Moore, J.C. (2018) Global streamflow and river discharge under stratospheric aerosol

geoengineering. *Atmospheric Chemistry and Physics*, 18, 16033–16050.

Werner, A.T. and Canon, A.J. (2016) Hydrologic extremes: an intercomparison of multiple gridded statistical downscaling methods. *Hydrology and Earth System Sciences*, 20(4), 1483–1508.

Wigley, T.M.L. (2006) A combined mitigation/geoengineering approach to climate stabilization. *Science*, 3144, 452–454.

Wolkoff, P. (2018) Indoor air humidity, air quality, and health: an overview. *International Journal of Hygiene and Environmental Health*, 22, 376–390.

Wood, A.W., Leung, L.R., Sridhar, V. and Lettenmaier, D.P. (2004) Hydrologic implications of dynamical and statistical approaches to downscaling climate model outputs. *Climate Change*, 62, 189–216.

Xia, L., Robock, A., Cole, J., Curry, C.L., Ji, D., Jones, A., Kravitz, B., Moore, J.C., Muri, H., Niemeier, U., Singh, B., Tilmes, S., Watanabe, S. and Yoon, J.-H. (2014) Solar radiation management impacts on agriculture in China: a case study in the geoengineering modelintercomparison project (GeoMIP). *Journal of Geophysical Research – Atmospheres*, 119(14), 8695–8711.

Yamanaka, M.D. (2016) Physical climatology of Indonesian maritime continent: an outline to comprehend observational studies. *Atmospheric Research*, 178-179, 231–259.

Yang, H., Dobbie, S., Vilegas, J.R., Feng, K., Challinor, A.J., Chen, B., Gao, Y., Lee, L., Yin, Y., Sun, L., Watson, J., Koehler, A.-K., Fan, T. and Ghost, S. (2016) Potential negative consequences of geoengineering on crop production: a study of Indian groundnut. *Geophysical Research Letters*, 43(22), 11786–11795.

Yu, X., More, J.C., Cui, X., Rinke, A., Ji, D., Kravitz, B. and Yoon, J.-H. (2015) Impacts, effectiveness and regional inequalities of the GeoMIP G1 to G4 solar radiation management scenarios. *Global and Planetary Change*, 129, 10–22.

Zhang, L., Xu, Y., Meng, C., Li, X., Liu, H. and Wang, G. (2020) Comparison of statistical and dynamic downscaling techniques in generating high-resolution temperatures in China from CMIP5 GCMs. *Journal of Applied Meteorology and Climatology*, 59(2), 207–235.

SUPPORTING INFORMATION

Additional supporting information may be found in the online version of the article at the publisher's website.